# Estimating Low-Latitude Scintillation Pattern Orientations and Irregularity Heights Using Measurements Made by a Local Array of Sensors

**Isaac G. Wright**, Josemaria Gomez Sócola, and Fabiano S. Rodrigues
The University of Texas at Dallas, W. B. Hanson Center for Space Sciences, Richardson, Texas

## 1. INTRODUCTION & MOTIVATION

- **Low-latitude scintillation is the manifestation of fast-moving and time-evolving diffraction patterns** created by ionospheric irregularities associated, in general, with Equatorial Spread-F (ESF).
- Theoretical and experimental studies of the orientation of scintillation fade patterns are **key to spaced-receiver scintillation analyses** and the interpretation of these measurements.
- It has been proposed that the orientation of these scintillation patterns can be determined from the **direction of the signal** and **the orientation of the magnetic field** (Kintner et al., 2004, Ledvina et al., 2004); however, modeling approaches failed whenever data were aligned within 60° of the magnetic field vector.

### 1.1 PROJECT GOALS

- **(G1) Revisit theoretical models** of scintillation pattern orientation and generalize them for more realistic receiver configurations.
- **(G2)** Conduct an experiment to **evaluate the results of our improved scintillation pattern model** with observed scintillation patterns.
- **(G3**) To investigate the ability of our model to **provide estimates of the height of the irregularities** responsible for observed scintillation**.**

## 2. METHODOLOGY

### 2.1 EXPERIMENTAL SETUP

- The study was conducted using **three low-cost scintillation monitors (ScintPi).** A ScintPi 3.0 is show in Figure 1 (Gomez Sócola and Rodrigues, 2022).
- The experiment was located at the Jicamarca Radio Observatory (JRO) from March 10-19, 2023, during ESF season. Jicamarca coordinates: 11.97° S, 76.87° W, ~0° dip latitude.
- **20 Hz multi-constellation, carrier to noise (C/No)** measurements were collected by monitors labeled T, O, and S, as shown in Figure 2.
- Monitors were located at different heights due to the terrain. Therefore, we operated not on the ground plane, but instead on a tilted surface which we refer to as the receiver plane.
- To correct this, we construct the **receiver coordinate system (RCS)**:
  - Contains two baselines approximately 964m in *y* and 140m in *x*.
- Coordinate frame transformations can be performed using the rotation matrix $R_{RCS}$ defined in terms of its unit axes as:

$$R_{RCS} = [\hat{x}_{RX} \quad \hat{y}_{RX} \quad \hat{z}_{RX}] \qquad (1)$$

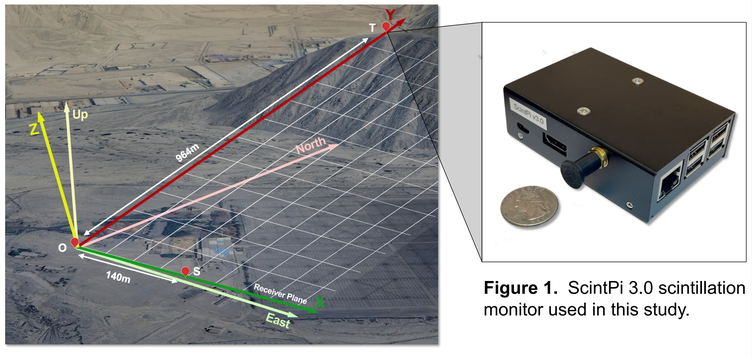




**Figure 1.** ScintPi 3.0 scintillation monitor used in this study.

**Figure 2.** (Left) Experiment array at the JRO. Receivers are labeled T, O, and S. Geographic ENU and RCS axes are shown in light and darker colors, respectively. From *Google Earth*.

### 2.2 MEASURING SCINTILLATION ORIENTATIONS

- As shown in Figure 3, the orientation of the scintillation pattern can be determined by modeling the scintillation pattern as a plane wave with velocity $\vec{v}$, projection angle $\phi$, and wavevector $\vec{k} = \langle \cos\phi\,, -\sin\phi \rangle$ and solving:

$$\vec{k} \cdot \vec{v} = \frac{\vec{a} \cdot \vec{k}}{\tau_a} = \frac{\vec{b} \cdot \vec{k}}{\tau_b} \qquad (2)$$

  Where $\vec{x}$ denotes the baseline vectors and $\tau_x$ the time lag (Kintner et al., 2004)
- C/No were **cross-correlated** between receiver pairs to obtain time lags.
- Data points were filtered for $S_4 > 0.2$, cross correlation magnitude $\rho_{max} > 0.7$, and elevation > 10°.
- To compare with the modeled angle (1), **we transform $\vec{q}$ to the receiver frame**, multiplying by *ENU* to *ECEF* and $R_{RCS}$ rotation matrices.

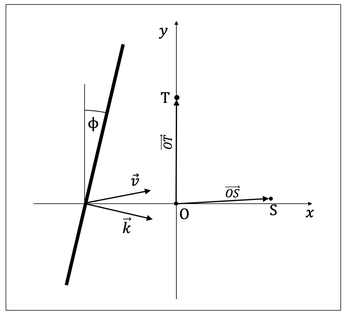


**Figure 3.** Scintillation fade pattern with normal vector $\vec{k}$ propagating with velocity $\vec{v}$ over receivers.

### 2.3 MODELING SCINTILLATION ORIENTATIONS

- Irregularities are thought to **elongate along the geomagnetic field line** (Farley, 1960). Therefore, knowing the satellite and receiver locations, and the ionospheric piercing point (IPP), **one can model the scintillation pattern orientation** on the ground.
- The scintillation pattern would be given by **the projection of $\vec{B}$ along $\vec{r}$**. This projection can be represented by a plane with normal vector $\vec{q}$ (Ledvina et al., 2004):

$$\vec{q} = \vec{r} \times \vec{B} \qquad (3)$$

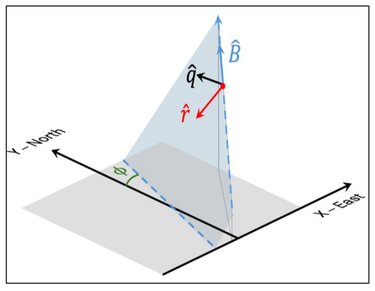


**Figure 4.** Illustration of projection geometry including the projection angle $\phi$. Note: Magnetic declination is nearly zero at JRO.

- **The intersection of the $\vec{q}$ plane and the *xy*-plane determines $\phi$,** as illustrated in Figure 4.
- $\vec{B}$ is obtained from IGRF-13 and assumes an IPP at 350 km altitude.

## 3. RESULTS

### 3.1 MODEL VALIDATIONS

- Projection angles measured by the local receiver array closely matched those predicted by our magnetic field projection model, as shown by Figure 5.
  - **Pearson R = 0.969,**
  - **Mean Absolute Error (MAE) = 1.47°**
- Observed projection angles spanned from -50° to +50°, showing **wide variability** even near the magnetic equator where the dip is approximately 0 °.
- **Strong agreement** between model and data supports the validity of the magnetic vector projection approach.

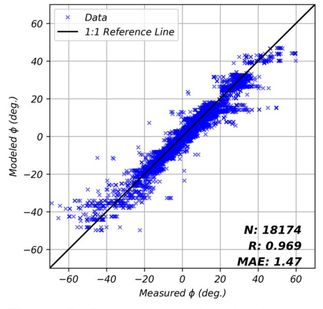


**Figure 5.** Comparison of projection angles obtained experimentally from the receiver array (measured $\phi$) and using the field-aligned model (modeled $\phi$).

### 3.2 SCATTERING HEIGHT ESTIMATES

- Model results assumed that the mean scattering height of irregularities contributing to scintillation occurred at 350 km.
- One can view the **scattering height as a free parameter** and attempt to estimate it by minimizing the MAE. This is done here, and results are shown in Figure 6.
- Minimum MAE values **align with the expected F-region peak near 350 km.**
- The curvature width in MAE plots can be interpreted as representing the **variability** in height throughout each night and scattering layer thickness.

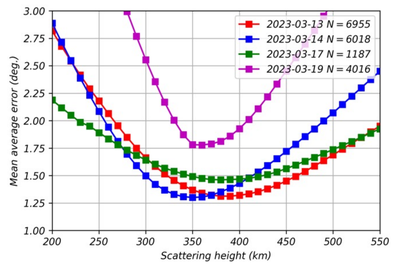


**Figure 6.** Height used in computation of $\vec{B}$ versus MAE for four days of the observation campaign.

## 4. DISCUSSIONS

- We hypothesize that the discrepancy observed in prior results (Kintner et al., 2004; see Figure 7) was due to approximating $\vec{B}$ by using only the value of $\vec{B}$ as that at the receiver array.
- In our approach, **$\vec{B}$ is obtained at each IPP.**
- This error is most prominent when $\vec{r}$ and $\vec{B}$ are aligned, as shown by the simulation results presented in Figure 8. This may explain why Kintner et al. (2004) found agreement only for data separated ≥60° from $\vec{B}$.

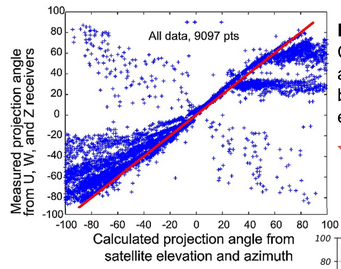


**Figure 7.** (Left) Comparison of projection angles originally observed by spaced array in Kintner et al. (2004).

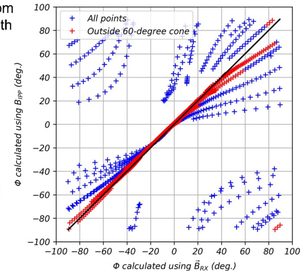


**Figure 8.** (Right) Simulation of how computed $\phi$ changes using $\vec{B}_{IPP}$ versus $\vec{B}_{RX}$ for a receiver array located at the low-latitude site of Cachoeira Paulista, Brazil and GPS ephemerides in 2001.

## 5. CONCLUSIONS

- **(G1)** We generalized the scintillation pattern orientation model proposed by Ledvina et al. (2004) to account for **projection onto a tilted surface,** which can represent more realistic situations of deployment and measurements.
- **(G2)** An array of low-cost, GNSS-based scintillation monitors **enabled us to measure projection angles of scintillation patterns**. The results are consistent with the proposed model, which will help interpretation of scintillation measurements.
- **(G3)** Using a model-measurement comparison (MAE) approach, we estimated the mean height of the irregularities causing observed scintillation. Results for different days show mean heights that are **consistent with the expectations of the F-region region peak height,** that is, 300 km to 400 km.

### ACKNOWLEDGEMENTS

We would like to thank the staff of the Jicamarca Radio Observatory for technical support. This material is based upon work supported by the NSF Graduate Research Fellowship Program under Grant No. (2136516), by NSF Award AGS-2122639, and by the Eugene McDermott Foundation.

### REFERENCES

Farley DT. 1960. Elec. fields in the iono. at non-polar geomag. latitudes. J. Geophys. Res. 65(3): 869–877.

Gomez Socola J, Rodrigues FS. 2022. ScintPi 2.0 and 3.0: GNSS-based monitors of ionospheric scintillation. EPS, 74, 185.

Kintner, P. M., B. M. Ledvina, E. R. de Paula, and I. J. Kantor (2004), Size, shape, orientation, speed.., Radio Sci.,39, RS2012.

Ledvina, B. M., P. M. Kintner, and E. R. de Paula (2004), Understanding spaced-receiver zonal velocity estimation, *J. Geophys. Res.*, 109, A10306